Available online at www.sciencedirect.com
ScienceDirect
Journal of Solid State Chemistry 181 (2008) 345–354
JOURNAL OF SOLID STATE CHEMISTRY
www.elsevier.com/locate/jssc

Syntheses, crystal structures and optical properties of the first strontium selenium(IV) and tellurium(IV) oxychlorides: $Sr_3(SeO_3)(Se_2O_5)Cl_2$ and $Sr_4(Te_3O_8)Cl_4$

Hai-Long Jiang[a,b], Jiang-Gao Mao[a,*]

[a]*State Key Laboratory of Structural Chemistry, Fujian Institute of Research on the Structure of Matter, Chinese Academy of Sciences, Fuzhou 350002, PR China*
[b]*Graduate School of the Chinese Academy of Sciences, Beijing 100039, PR China*

Received 13 November 2007; received in revised form 11 December 2007; accepted 12 December 2007

Abstract

Two new quaternary strontium selenium(IV) and tellurium(IV) oxychlorides, namely, $Sr_3(SeO_3)(Se_2O_5)Cl_2$ and $Sr_4(Te_3O_8)Cl_4$, have been prepared by solid-state reaction. $Sr_3(SeO_3)(Se_2O_5)Cl_2$ features a three-dimensional (3D) network structure constructed from strontium(II) interconnected by Cl^-, SeO_3^{2-} as well as $Se_2O_5^{2-}$ anions. The structure of $Sr_4(Te_3O_8)Cl_4$ features a 3D network in which the strontium tellurium oxide slabs are interconnected by bridging Cl^- anions. The diffuse reflectance spectrum measurements and results of the electronic band structure calculations indicate that both compounds are wide band-gap semiconductors.

Keywords: Strontium(II) Se(IV) or Te(IV) oxychloride; Solid-state reaction; Crystal structure; Band structure; Optical properties

1. Introduction

Metal selenites and tellurites can adopt a variety of structures due to the presence of the lone-pair electrons that could serve as an invisible structure-directing agent [1,2]. These lone-pair electrons may also aid in the formation of asymmetric coordination environments for metal centers, resulting in the possible noncentrosymmetric (NCS) structures with consequent interesting physical properties, such as second harmonic generation (SHG), piezoelectricity, pyroelectricity and ferroelectricity [3–15]. Furthermore, transition metal Se(IV) or Te(IV) oxyhalides can be regarded as "chemical scissors" and they can be promising new low-dimensional magnets [16–19].

Comparing with transition metal selenites or tellurites [16–27], the corresponding alkaline earth (AE) or alkali metal compounds normally display larger band gaps, also a few of them display excellent SHG properties, such as $Na_2TeW_2O_9$ and $BaTeM_2O_9$ (M = Mo, W) [4–6]. From recent report, it is interesting to note that a possible giant enhancement of the second-order optical properties of the Sr-containing crystallites occurred because of the nanocrystallites with sizes of about 100–250 nm [28]. Although a few alkali metal or AE selenites and tellurium(IV) oxides have been reported [4,5,13,14,29,30], reports on AE selenites and tellurium(IV) oxides with additional halide anions are still rare [31–35]. Up to now, only six AE selenium(IV) or tellurium(IV) oxyhalides, namely, $Ba_2CoCl_2(SeO_3)_2$, $Ba_3(TeO_3)_2Cl_2$, $Ba_2Cu_4Te_4O_{11}Cl_4$, $BaCu_2Te_2O_6Cl_2$, $Sr_2Cu_2TeO_6Br_2$ and $Ca_2CuTe_4O_{10}Cl_2$, have been synthesized and structurally characterized, most of them containing a transition metal [31–35]. Due to the large difference in the bond distances between AE–O and AE–Cl, the introduction of halide anion into the AE selenium(IV) or tellurium(IV) oxide systems may enhance the possibility to obtain compounds with acentric structures. Our research efforts on new optical materials in the unexplored Sr–Se^{IV}(Te^{IV})–O–Cl systems yielded two new strontium selenium(IV) and tellurium(IV) oxychlorides, namely, $Sr_3(SeO_3)(Se_2O_5)Cl_2$ and $Sr_4(Te_3O_8)Cl_4$. Herein, we report their syntheses, crystal and band structures and optical properties.

*Corresponding author. Fax: +86 591 8371 4946.
E-mail address: mjg@fjirsm.ac.cn (J.-G. Mao).

0022-4596/$ - see front matter © 2008 Elsevier Inc. All rights reserved.
doi:10.1016/j.jssc.2007.12.007

2. Experimental section

2.1. Materials and instrumentation

Analytically pure ZnO, $SrCO_3$ and $SrCl_2 \cdot 2H_2O$ were purchased from the Shanghai Reagent Factory; SeO_2 (99 + %) and TeO_2 (99 + %) were bought from ACROS ORGANICS. SrO was synthesized by heating $SrCO_3$ in air at 1050 °C for 10 h. $SrCl_2 \cdot 2H_2O$ was heated in air at 160 °C overnight before used in order to dehydrate. Infrared (IR) spectra were recorded on a Magna 750 Fourier-transform IR (FT–IR) spectrometer photometer as a KBr pellet in the 4000–400 cm^{-1}. Microprobe elemental analyses on Sr, Te, Se and Cl elements were performed on a field emission scanning electron microscope (FESEM, JSM6700F) equipped with an energy dispersive X-ray spectroscope (EDS, Oxford INCA). X-ray powder diffraction (XRD) patterns (Cu $K\alpha$) were collected on a XPERT-MPD θ–2θ diffractometer. Optical diffuse reflectance spectra were measured at room temperature with a PE Lambda 900 ultraviolet (UV)–vis spectrophotometer. The instrument was equipped with an integrating sphere and controlled by a personal computer. The samples were ground into fine powder and pressed onto a thin glass slide holder. $BaSO_4$ plate was used as a standard (100% reflectance). The absorption spectra were calculated from reflectance spectra using the Kubelka–Munk function: $\alpha/S = (1-R)^2/2R$ [36], where α is the absorption coefficient, S is the scattering coefficient which is practically wavelength independent when the particle size is larger than 5 μm, and R is the reflectance. Thermogravimetric analyses (TGA) were carried out with a NETZSCH STA 449C unit, at a heating rate of 10 °C/min under a static air atmosphere.

2.2. Preparation of $Sr_3(SeO_3)(Se_2O_5)Cl_2$

Colorless needle-shaped single crystals of $Sr_3(SeO_3)(Se_2O_5)Cl_2$ were initially obtained in our attempt to prepare a Sr–Zn–SeO_3–Cl phase by solid-state reaction of 1.2 mmol of $SrCl_2$ (0.190 g), 1.2 mmol of ZnO (0.098 g) and 1.2 mmol SeO_2 (0.133 g) in an evacuated quartz tube at 660 °C for 6 days and then cooled to 300 °C at 3 °C/h before switching off the furnace. Results of EDS microprobe elemental analyses on single crystals of $Sr_3(SeO_3)(Se_2O_5)Cl_2$ gave molar ratio of Sr:Se:Cl of 2.8:3.3:1.0, no Zn element was detected. After proper structural determination, a pure powder sample of $Sr_3(SeO_3)(Se_2O_5)Cl_2$ was prepared quantitatively by solid-state reaction of a mixture composed of SrO, $SrCl_2$ and SeO_2 in a molar ratio of 2:1:3 at 660 °C. Its purity was confirmed by XRD studies (see Supporting Materials). IR data (KBr cm^{-1}): 874 (m), 851 (m), 821 (vs.), 776 (vs.), 718 (s), 670 (s), 636 (s), 559 (m), 463 (w) and 437 (m).

2.3. Preparation of $Sr_4(Te_3O_8)Cl_4$

Single crystals of $Sr_4(Te_3O_8)Cl_4$ were initially prepared by the solid-state reaction of a mixture containing 0.4 mmol of $SrCl_2$ (0.063 g), 0.8 mmol of SrO (0.083 g) and 1.2 mmol of TeO_2 (0.192 g). The reaction mixture was thoroughly ground and pressed into a pellet, which was then put into quartz tube, evacuated and sealed. The quartz tube was heated at 660 °C for 6 days and then cooled to 300 °C at 4 °C/h before switching off the furnace. The measured molar ratio of Sr:Te:Cl by microprobe elemental analysis is 4.0:2.8:4.3, which is in good agreement with the one determined from single-crystal X-ray structural analysis. After the structural analysis, a pure powder sample of $Sr_4(Te_3O_8)Cl_4$ was prepared quantitatively by reacting a mixture of SrO, $SrCl_2$ and TeO_2 in a molar ratio of 2:2:3 at 720 °C for 6 days. Its purity was confirmed by XRD studies (see Supporting Materials). IR data (KBr cm^{-1}): 763(vs.), 698(vs.), 586(s), 447(w) and 411(m).

2.4. Single-crystal structure determination

Data collections for both compounds were performed on a Rigaku mercury CCD diffractometer equipped with a graphite-monochromated Mo–$K\alpha$ radiation ($\lambda = 0.71073$ Å) at 293 K. The data sets were corrected for Lorentz and polarization factors as well as for absorption by multi-scan method [37]. Both structures were solved by the direct methods and refined by full-matrix least squares fitting on F^2 by SHELX-97 [38]. All atoms were refined with anisotropic thermal parameters. Cl(5) in $Sr_4(Te_3O_8)Cl_4$ is disordered over two orientations ((0.5000, 0.5567, 0) and (0.5000, 0.4433, 0)) related by a mirror plane, which are close to the 2/m symmetry site with an interatomic distance of 0.6522 Å. Hence, its occupancy factor is reduced by 50%. Data collection and refinement parameters are summarized in Table 1. Selected bond lengths and bond angles are listed in Table 2. Further details of the crystal structure investigations can be obtained from the Fachinformationszentrum Karlsruhe, 76344 Eggenstein-Leopoldshafen, Germany (fax: (49) 7247-808-666; e-mail: crysdata@fiz-karlsruhe.de), on quoting the depository numbers CSD–418542 and 418557.

2.5. Computational details

Single-crystal structural data of the two compounds were used for the theoretical calculations. As mentioned before, the Cl(5) atom in $Sr_4(Te_3O_8)Cl_4$ was disordered over two orientations close to the 2/m site, the ideal structural model with Cl(5) positioned at the 2/m site (0.5000, 0.5000, 0) was used for the calculations. Band structure and optical property calculations were performed with the total-energy code CASTEP [39–41]. The total energy is calculated with density functional theory (DFT) using Perdew–Burke–Ernzerhof generalized gradient approximation [42]. The interactions between the ionic cores and the electrons are described by the norm-conserving pseudopotential [43,44]. The following orbital electrons are treated as valence electrons: Sr-$4s^2 4p^6 5s^2$, Te-$5s^2 5p^4$, Se-$4s^2 4p^4$, Cl-$3s^2 3p^5$ and O-$2s^2 2p^4$. Considering the balance of computational cost and precision, a cutoff energy of 450 eV and a $2 \times 4 \times 1$

Table 1
Crystal data and structure refinements for $Sr_3(SeO_3)(Se_2O_5)Cl_2$ and $Sr_4(Te_3O_8)Cl_4$

Formula	$Sr_3Se_3Cl_2O_8$	$Sr_4Te_3Cl_4O_8$
Formula weight	698.64	1003.08
Space group	P*nma* (No. 62)	C2/*m* (No.12)
a(Å)	11.5538(17)	16.301(2)
b (Å)	5.5333(9)	5.7469(5)
c (Å)	17.366(3)	17.109(2)
α (°)	90	90
β (°)	90	109.648(4)
γ (°)	90	90
V(Å^3)	1110.2(3)	1509.5(3)
Z	4	4
D_{calc}(g cm^3)	4.180	4.414
μ(Mo$K\alpha$)(mm^{-1})	24.697	20.471
Crystal size(mm)	0.35 × 0.03 × 0.02	0.20 × 0.05 × 0.03
F(000)	1256	1760
Reflections collected	8270	5866
Independent reflections	1413 (R_{int} = 0.0687)	1900 (R_{int} = 0.0410)
Observed data[$I>2\sigma(I)$]	1268	1501
Data/restraints/ parameters	1413/0/88	1900/0/109
GOF on F^2	1.274	1.105
R_1, wR_2 ($I>2\sigma(I)$)[a]	0.0552, 0.0899	0.0417, 0.0897
R_1, wR_2 (all data)	0.0656, 0.0931	0.0560, 0.0970

[a] $R_1 = \text{Å}||F_o|-|F_c||/\text{Å}|F_o|$, $wR_2 = \{\text{Å}w[(F_o)^2-(F_c)^2]^2/\text{Å}w[(F_o)^2]^2\}^{1/2}$.

Monkhorst–Pack k-point sampling were used for $Sr_3(SeO_3)(Se_2O_5)Cl_2$, and a cutoff energy of 450 eV and a $4\times4\times1$ Monkhorst–Pack k-point sampling for $Sr_4(Te_3O_8)Cl_4$. The 36 and 12 empty bands are used for the calculations of optical properties for $Sr_3(SeO_3)(Se_2O_5)Cl_2$ and $Sr_4(Te_3O_8)Cl_4$, respectively. The other calculating parameters and convergent criteria are the default values of CASTEP code.

The calculations of linear optical properties were also made in this work. The imaginary part of the dielectric function, $\varepsilon_2(\omega)$, is given by the following equation:

$$\varepsilon_2(q\rightarrow O_{\hat{u}},\hbar\omega)=\frac{2e^2\pi}{\Omega\varepsilon_0}\sum_{k,v,c}\left|\left\langle\Psi_k^c\right|\left|\hat{u}r\right\rangle\Psi_k^v\right|^2\times\delta(E_k^c-E_k^v-E), \quad (1)$$

where c and v are band indexes, Ω is the volume of the system, and $\hat{u}$ is the vector defining the polarization of the incident electric field. $\varepsilon_2(\omega)$ can be thought of as detailing the real transitions between occupied and unoccupied electronic states. Since the dielectric constant describes a causal response, the real and imaginary parts are linked by a Kramers–Kronig transform [45].

$$\varepsilon_1(\omega)-1=P\frac{2}{\pi}\int_0^\infty\frac{\omega'\varepsilon_2(\omega')\,d\omega'}{\omega'^2-\omega^2},$$
$$\varepsilon_2(\omega)=-\frac{2\omega}{\pi}P\int_0^\infty\frac{\varepsilon_1(\omega')\,d\omega'}{\omega'^2-\omega^2}, \quad (2)$$

where P means the principal value of the integral. This transform is used to obtain the real part of the dielectric function, $\varepsilon_1(\omega)$.

Table 2
Selected bond lengths (Å) and angles (°) for $Sr_3(SeO_3)(Se_2O_5)Cl_2$ and $Sr_4(Te_3O_8)Cl_4$

$Sr_3(SeO_3)(Se_2O_5)Cl_2$			
Sr(1)–O(1)#1	2.532(5)	Sr(1)–O(1)#2	2.532(6)
Sr(1)–O(3)	2.534(6)	Sr(1)–O(3)#3	2.534(6)
Sr(1)–O(4)	2.567(8)	Sr(1)–Cl(1)#4	2.994(3)
Sr(1)–Cl(1)#5	3.081(1)	Sr(1)–Cl(1)	3.081(1)
Sr(2)–O(5)	2.555(5)	Sr(2)–O(5)#6	2.555(6)
Sr(2)–O(3)#6	2.657(6)	Sr(2)–O(3)	2.657(6)
Sr(2)–O(5)#7	2.685(6)	Sr(2)–O(5)#8	2.685(6)
Sr(2)–O(4)	2.935(3)	Sr(2)–O(4)#9	2.935(3)
Sr(2)–Cl(1)	3.045(3)	Sr(3)–O(2)	2.913(3)
Sr(3)–O(5)#10	2.580(5)	Sr(3)–O(5)#8	2.580(5)
Sr(3)–O(1)	2.732(6)	Sr(3)–O(1)#3	2.732(6)
Sr(3)–O(3)#3	2.776(6)	Sr(3)–O(3)	2.776(6)
Sr(3)–O(2)#5	2.913(3)	Sr(3)–Cl(2)	3.102(3)
Sr(3)–Cl(2)#11	3.276(4)		
Se(1)–O(1)	1.651(6)	Se(1)–O(1)#6	1.651(6)
Se(1)–O(2)	1.818(8)	Se(2)–O(2)	1.818(9)
Se(2)–O(3)	1.665(5)	Se(2)–O(3)#6	1.665(5)
Se(3)–O(4)	1.681(8)	Se(3)–O(5)	1.695(6)
Se(3)–O(5)#3	1.695(6)		
O(1)#6–Se(1)–O(1)	105.4(4)	O(1)#6–Se(1)–O(2)	93.5(3)
O(1)–Se(1)–O(2)	93.5(3)	O(3)–Se(2)–O(3)#6	100.5(4)
O(3)–Se(2)–O(2)	93.7(3)	O(3)#6–Se(2)–O(2)	93.7(3)
O(4)–Se(3)–O(5)	100.5(3)	O(4)–Se(3)–O(5)#3	100.5(3)
O(5)–Se(3)–O(5)#3	98.8(4)		
$Sr_4(Te_3O_8)Cl_4$			
Sr(1)–O(1)#1	2.589(5)	Sr(1)–O(1)	2.589(5)
Sr(1)–O(3)	2.633(5)	Sr(1)–O(3)#1	2.633(5)
Sr(1)–O(2)#2	2.657(5)	Sr(1)–O(2)#3	2.657(5)
Sr(1)–Cl(2)	2.984(4)	Sr(1)–O(5)#4	3.045(3)
Sr(1)–O(5)	3.045(3)	Sr(2)–O(1)#6	2.545(5)
Sr(2)–O(1)#7	2.545(5)	Sr(2)–O(2)#8	2.634(5)
Sr(2)–O(2)#2	2.634(5)	Sr(2)–O(1)	2.654(5)
Sr(2)–O(1)#9	2.654(5)	Sr(2)–Cl(3)	3.055(1)
Sr(2)–O(4)#2	3.068(3)	Sr(2)–O(4)#5	3.068(3)
Sr(3)–O(2)	2.527(5)	Sr(3)–O(2)#1	2.527(5)
Sr(3)–O(3)#10	2.726(6)	Sr(3)–O(3)#11	2.726(6)
Sr(3)–Cl(5)#12	2.942(2)	Sr(3)–Cl(5)	2.942(2)
Sr(3)–Cl(1)#6	3.087(1)	Sr(3)–Cl(1)#13	3.087(1)
Sr(3)–Cl(2)	3.091(4)	Sr(4)–O(3)#1	2.488(5)
Sr(4)–O(3)	2.488(5)	Sr(4)–Cl(4)	2.900(6)
Sr(4)–Cl(1)#14	2.940(3)	Sr(4)–Cl(1)#15	3.183(4)
Sr(4)–Cl(4)#16	3.284(3)	Sr(4)–Cl(4)#17	3.284(3)
Sr(4)–Cl(5)#2	3.342(7)	Sr(4)–Cl(5)#17	3.342(7)
Te(1)–O(1)#9	1.851(5)	Te(1)–O(1)	1.851(5)
Te(1)–O(5)	2.114(8)	Te(1)–O(4)#18	2.130(9)
Te(2)–O(2)#1	1.851(5)	Te(2)–O(2)#19	1.851(5)
Te(2)–O(4)	1.869(9)	Te(3)–O(3)#9	1.859(5)
Te(3)–O(3)	1.859(5)	Te(3)–O(5)	1.896(8)
O(1)#9–Te(1)–O(1)	96.5(3)	O(1)#9–Te(1)–O(5)	85.9(2)
O(1)–Te(1)–O(5)	85.9(2)	O(1)#9–Te(1)–O(4)#18	86.7(2)
O(1)–Te(1)–O(4)#18	86.7(2)	O(5)–Te(1)–O(4)#18	168.9(4)
O(2)#1–Te(2)–O(2)#19	95.4(3)	O(2)#1–Te(2)–O(4)	94.0(2)
O(2)#19–Te(2)–O(4)	94.0(2)	O(3)#9–Te(3)–O(3)	93.9(3)
O(3)#9–Te(3)–O(5)	93.1(2)	O(3)–Te(3)–O(5)	93.1(2)

Symmetry transformations used to generate equivalent atoms: for $Sr_3(SeO_3)(Se_2O_5)Cl_2$: #1: $x+1/2$, y, $-z+1/2$; #2: $x+1/2$, $-y+3/2$, $-z+1/2$; #3: x, $-y+3/2$, z; #4: $-x+2$, $-y+1$, $-z+1$; #5: x, $y+1$, z; #6: x, $-y+1/2$, z; #7: $-x+1$, $y-1/2$, $-z+1$; #8: $-x+1$, $-y+1$, $-z+1$; #9: x, $y-1$, z; #10: $-x+1$, $y+1/2$, $-z+1$; #11: $x-1/2$, y, $-z+1/2$.
For $Sr_4(Te_3O_8)Cl_4$: #1: x, $-y+1$, z; #2: $x-1/2$, $y-1/2$, z; #3: $x-1/2$, $-y+3/2$, z; #4: x, $y+1$, z; #5: $x-1/2$, $y+1/2$, z; #6: $-x+1/2$, $-y+1/2$, $-z+1$; #7: $-x+1/2$, $y-1/2$, $-z+1$; #8: $x-1/2$, $-y+1/2$, z; #9: x, $-y$, z; #10: $x+1/2$, $y+1/2$, z; #11: x+1/2, $-y+1/2$, z; #12: $-x+1$, $-y+1$, $-z$; #13: $-x+1/2$, $-y+3/2$, $-z+1$; #14: x, y, $z-1$; #15: $-x$, $-y+1$, $-z+1$; #16: $-x+1/2$, $-y+1/2$, $-z$; #17: $-x+1/2$, $-y+3/2$, $-z$; #18: $-x+1$, $-y$, $-z+1$; #19: x,$y-1$,z.

3. Results and discussion

Solid-state reactions of strontium oxide, strontium chloride and SeO_2 or TeO_2 at high temperature led to two new quaternary compounds, namely, $Sr_3(SeO_3)(Se_2O_5)Cl_2$ and $Sr_4(Te_3O_8)Cl_4$. They represent the first examples of strontium selenium(IV) and tellurium(IV) oxyhalides.

3.1. Crystal structure of $Sr_3(SeO_3)(Se_2O_5)Cl_2$

The synthesis of $Sr_3(SeO_3)(Se_2O_5)Cl_2$ can be expressed by the following reaction at 660 °C:$2SrO + SrCl_2 + 3SeO_2 \rightarrow Sr_3(SeO_3)(Se_2O_5)Cl_2$. Its structure features a three-dimensional (3D) network built by strontium(II) cations being interconnected by Cl^-, SeO_3^{2-} as well as $Se_2O_5^{2-}$ anions (Fig. 1). The asymmetric unit of $Sr_3(SeO_3)(Se_2O_5)Cl_2$ contains three unique strontium(II) cations, three selenite anions and two chloride anions. Sr(1) is 8-coordinated by five selenite oxygens and three chloride anions, and Sr(2) is 9-coordinated by eight selenite oxygens and one chloride anion whereas Sr(3) is 10-coordinated by eight selenite oxygen and two chloride anions. The Sr–Cl distances (2.994(3)–3.276(4) Å) are significantly longer than those of the Sr–O bonds (2.532(5)–2.935(3) Å) (Table 2), the corresponding chemical bonds are determined by s-Sr-3pCl (or 2p-O) charge transfer with mainly ionic character (see also theoretical study section). These Sr–O and Sr–Cl distances are comparable to those reported in other strontium compounds [46,47]. All selenium(IV) atoms are 3-coordinated by three oxygen atoms in a distorted ψ-SeO_3 trigonal pyramidal geometry with the pyramidal site occupied by the lone pair of Se(IV). The Se–O distances fall in the range of 1.651(6)–1.818(9) Å and the O–Se–O bond angles range from 93.5(3) to 105.4(4), which are comparable to those reported in other metal selenites [1,2]. Results of bond valence calculations indicate that the strontium and selenium atoms are in +2 and +4 oxidation states, respectively [48,49]. The calculated total bond valences are 2.30, 1.97, 1.85, 4.06, 3.95 and 4.16, respectively, for Sr(1), Sr(2), Sr(3), Se(1), Se(2) and Se(3).

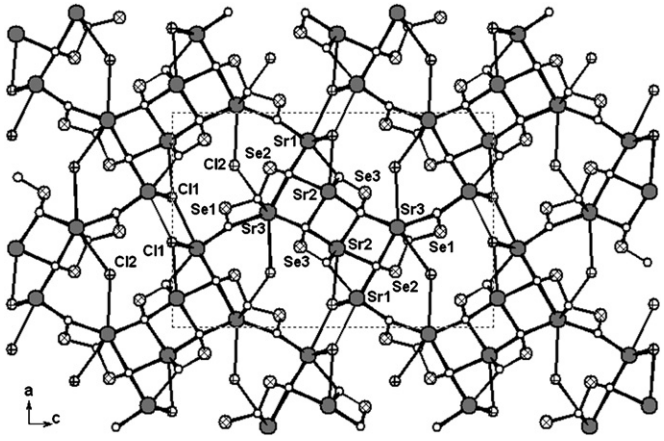

Fig. 1. View of the structure of $Sr_3(SeO_3)(Se_2O_5)Cl_2$ down the *b*-axis. Sr, Se, Cl and O atoms are represented by medium gray, hatched, crossed and open circles, respectively.

$Se(1)O_3$ and $Se(2)O_3$ groups are interconnected via corner-sharing (O(2)) into a diselenite anion ($Se_2O_5^{2-}$). It is dodecadentate, tridentately chelating with two Sr(3) (O(1), O(2) and O(3)), bidentately chelating with a Sr(2) (O(3)) and also bridging with four Sr(1) atoms. O(3) is tridentate whereas O(1) and O(2) are bidentate. The $Se(3)O_3$ group is nonadentate, chelating bidentately with three Sr(2) atom and also bridging with one Sr(1) and two Sr(3) atoms. All three selenite oxygens are tridentate metal linkers (Scheme 1).

The Sr^{2+} ions are interconnected by SeO_3^{2-} and $Se_2O_5^{2-}$ anions via Se–O–Sr bridges into a 3D open-framework of $[Sr_3Se_3O_8]^{2+}$ with 12 member-ring (MR) tunnels running to *b*-axis (see Supporting Materials). The Cl^- anions are located at the above 12-MR tunnels, which greatly reduced the voids of the 3D structure (Fig. 1).

It is worthy to note that the strontium(II) ions are bridged by Cl(1) and Cl(2) anions into two types of chains (Fig. 2). Cl(1) bridges one Sr(2) and three Sr(1) atoms into a double chain whereas Cl(2) bridges two Sr(3) atoms into a wave-like strontium chloride chain.

The 3D network of $Sr_3(SeO_3)(Se_2O_5)Cl_2$ can also be viewed as formed by the interconnection of strontium(II) ions by bridging Cl^-, SeO_3^{2-} as well as $Se_2O_5^{2-}$ anions, lone-pair electrons of the Se^{4+} ions are orientated toward the

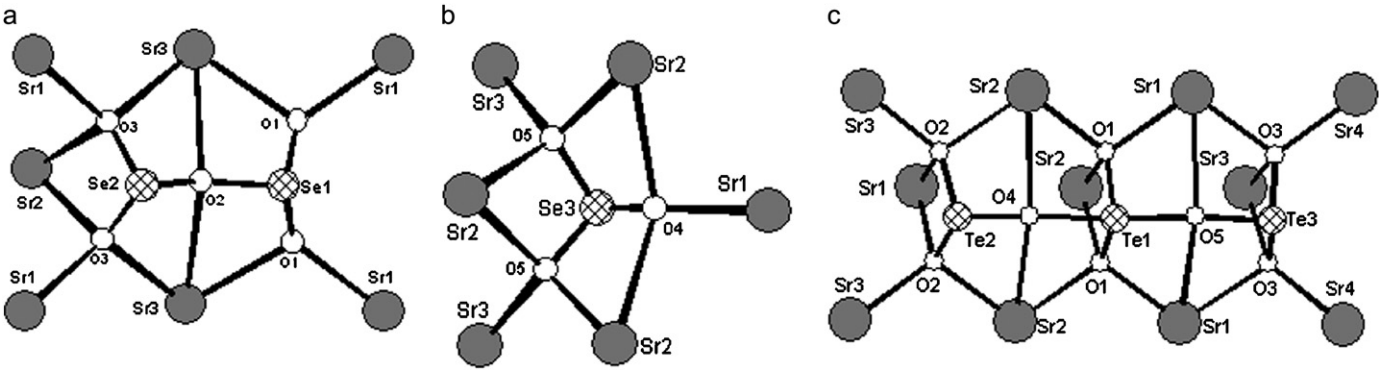

Scheme 1. The coordination modes of $Se_2O_5^{2-}$ (a) and SeO_3^{2-} (b) anions in $Sr_3(SeO_3)(Se_2O_5)Cl_2$ and $Te_3O_8^{4-}$ (c) in $Sr_4(Te_3O_8)Cl_4$.

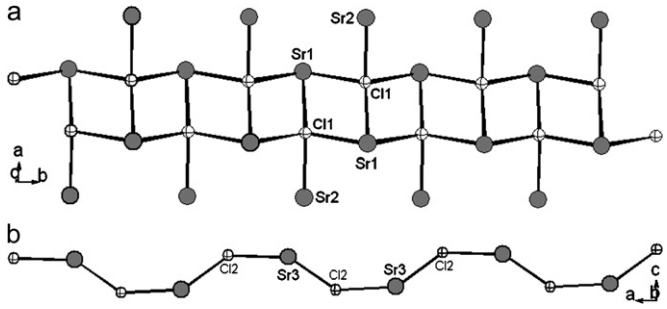

Fig. 2. (a) A 1D strontium chloride double chain along the *b*-axis (b) A 1D strontium chloride chain along the *a*-axis.

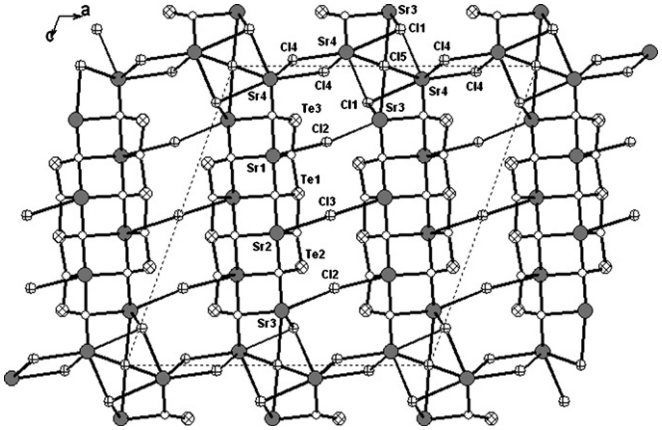

Fig. 3. View of the structure of $Sr_4(Te_3O_8)Cl_4$ down the *b*-axis. Sr, Te, Cl and O atoms are represented by medium gray, hatched, crossed and open circles, respectively.

voids of the structure (Fig. 1). The effective volume of the lone-pair electrons is approximately the same as the volume of an O^{2-} anion according to Galy and Andersson [50].

3.2. Crystal structure of $Sr_4(Te_3O_8)Cl_4$

The synthesis of $Sr_4(Te_3O_8)Cl_4$ can be expressed by the following reaction at 720 °C: $2SrO + 2SrCl_2 + 3TeO_2 \rightarrow Sr_4(Te_3O_8)Cl_4$. Its structure features a 3D network constructed by one-dimensional (1D) strontium tellurium(IV) oxide slabs interconnected by bridging chloride anions (Fig. 3). The asymmetric unit of $Sr_4(Te_3O_8)Cl_4$ contains four strontium(II) cations, four chloride anions and a $Te_3O_8^{4-}$ anion. Both Sr(1) and Sr(2) are 9-coordinated by eight tellurite oxygens and one chloride anion, Sr(3) is 8-coordinated by four tellurite oxygens and four chloride anions whereas Sr(4) is 8-coordinated by two tellurite oxygens and six chloride anions. The Sr–Cl distances (2.900(6)–3.342(7) Å) are significantly longer than those of the Sr–O bonds (2.488(5)–3.068(3) Å), these distances are comparable to those in $Sr_3(SeO_3)(Se_2O_5)Cl_2$ and other strontium compounds [46,47]. Te(1) is coordinated by four oxygen atoms in a distorted ψ-TeO_4 tetragonal pyramidal geometry with the fifth site occupied by the lone-pair electrons of the Te(IV) whereas, Te(2) and Te(3) are coordinated by three oxygen atoms in a distorted ψ-TeO_3 trigonal pyramidal geometry with pyramidal site occupied by the lone-pair electrons. The TeO_4 and TeO_3 groups are interconnected by two Te–O–Te bridges into a linear trinuclear $(Te_3O_8)^{4-}$ anion. The O–Te–O bond angles range from 85.9(2)° to 168.9(4)°, which are comparable to those reported in other metal tellurites [1,2]. Results of bond valence calculations indicate that all strontium and tellurium atoms are in +2 and +4 oxidation states, respectively [48,49]. The calculated total bond valences are 1.96, 1.98, 2.30, 2.02, 4.16, 4.15 and 4.00, respectively, for Sr(1), Sr(2), Sr(3), Sr(4), Te(1), Te(2) and Te(3).

Each $Te_3O_8^{4-}$ anion connects with 11 Sr^{2+} cations, it forms four Sr–O–Te–O–Te–O six member chelation rings and three Sr–O–Te–O four member chelation rings and also bridges with four other Sr(II) ions. O(1), O(2) and O(3) are tridentate metal linkers whereas O(4) and O(5) are only involved in the formation of the Te–O–Te bridges (Scheme 1). Such kind of connectivity leads to a thick strontium tellurium(IV) oxide slab with a width of about 14.8 Å (Fig. 4(a)).

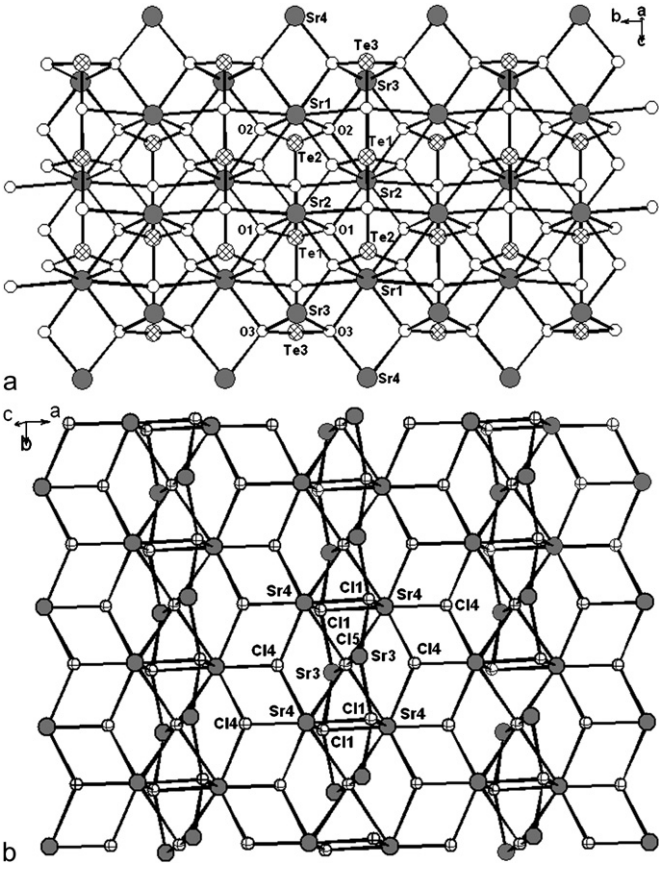

Fig. 4. A 1D strontium tellurium(IV) oxide slab along the *b*-axis (a) and a 2D strontium chloride layer parallel to the *ab*-plane in $Sr_4(Te_3O_8)Cl_4$ (b). Sr, Te, Cl and O atoms are represented by medium gray, hatched, crossed and open circles, respectively.

It is interesting to note that Sr(3) and Sr(4) cations are bridged by Cl(1), Cl(4) and Cl(5) anions into a 2D strontium chloride layer parallel to the *ab*-plane (Fig. 4(b)). Such two-dimensional (2D) layer can also be viewed as 1D chains of Sr_6 octahedra along the *b*-axis which are interconnected by tridentate Cl(4) atoms, the other chloride anions act as bridging atoms of the Sr…Sr edges or as capping atoms on the Sr_3 triangles. The Sr…Sr separations range from 4.275(1) to 5.747(1) Å.

The above 1D strontium tellurium (IV) oxide slabs are bridged by Cl(2) and Cl(3) atoms along *a*-axis into a thick strontium tellurium(IV) oxychloride layer parallel to the *ab*-plane. Along the ⟨001⟩ direction, the above 2D layers are further interconnected by the 2D strontium chloride sheets into a complicated 3D network of $Sr_4(Te_3O_8)Cl_4$ (Fig. 3). The lone-pair electrons of the Te(IV) ions are orientated toward the voids of the structure.

It is also worthy to mention the connectivity of the selenium(IV) and tellurium(IV) oxides anions. The selenium(IV) atom is usually only coordinated by three oxygens, and two SeO_3^{2-} anions can form a $Se_2O_5^{2-}$ anion through a Se–O–Se bridge. It is uncommon for the SeO_3^{2-} and $Se_2O_5^{2-}$ anions to be present within a same compound. A CSD search indicates that only eight compounds, namely, $Ca_2(SeO_3)(Se_2O_5)$ [51], $Au_2(SeO_3)_2(Se_2O_5)$ [52], $MnH(SeO_3)(Se_2O_5)$ [53], $PrH_3(SeO_3)_2(Se_2O_5)$ [54], $M(SeO_3H))(Se_2O_5)$ (M = Cr, Fe) [55,56], $Ga(HSeO_3)(Se_2O_5)(H_2O)_{1.075}$ [57] and $Nd_2(Se_2O_5)_3(H_2SeO_3)(H_2O)_2$ [58], contain both $Se_2O_5^{2-}$ and SeO_3^{2-} (or $HSeO_3^-$ or H_2SeO_3). The tellurium(IV) atom in combination with oxygen atoms can form a number of isolated polynuclear anionic units and polynuclear anions with extended structures due to the polymerization of the TeO_x (x = 3,4,5) groups [26,59–64].

3.3. Thermogravimetric analyses (TGA)

TGA curves indicate that $Sr_3(SeO_3)(Se_2O_5)Cl_2$ and $Sr_4(Te_3O_8)Cl_4$ are stable up to about 475 and 540 °C (Fig. 5), respectively. $Sr_3(SeO_3)(Se_2O_5)Cl_2$ exhibits two main steps of weight losses. The first one occurred in the temperature range of 475–650 °C that corresponds to the release of one SeO_2. The observed weight loss of 16.0% is close to the calculated value (15.9%). Then it exhibits a plateau in the approximate range of 650–770 °C. Above 770 °C, it is further decomposed. The total weight loss at 1300 °C is 46.6% and the final residues were not characterized. $Sr_4(Te_3O_8)Cl_4$ only exhibits one main step of weight loss and it decomposes continuously up to 1300 °C, which probably corresponds to the release of TeO_2 and Cl_2. The observed total weight loss is 23.2%. The final residuals are not characterized due to its reaction with the TGA buckets (made of Al_2O_3) under such high temperatures.

3.4. IR and optical spectrum studies

IR studies indicate that both $Sr_3(SeO_3)(Se_2O_5)Cl_2$ and $Sr_4(Te_3O_8)Cl_4$ are transparent in the range of 4000–1000 cm^{-1}. The absorption bands of $Sr_3(SeO_3)(Se_2O_5)Cl_2$ at 874, 851, 821, 776 and 718 cm^{-1} can be assigned to the ν(Se–O) vibrations, and those at 463, 454, 436 and 403 cm^{-1} can be attributed to the ν(O–Se–O) vibrations, whereas those at 670, 656, 559 cm^{-1} originate from the ν(Se–O–M) vibrations. The absorption bands of $Sr_4(Te_3O_8)Cl_4$ at 763, 698 and 586 cm^{-1} are characteristic of the ν(Te–O) vibrations, and bands at 411 and 447 cm^{-1} are due to the ν(Te–O–M) vibrations. All of the assignments are consistent with those reported in related compounds [65,66]. Optical diffuse reflectance spectra of $Sr_3(SeO_3)(Se_2O_5)Cl_2$ and $Sr_4(Te_3O_8)Cl_4$ reveal optical band gaps of 4.4 and 4.0 eV, respectively (Fig. 6). Hence, both the compounds are wide band gap semiconductors.

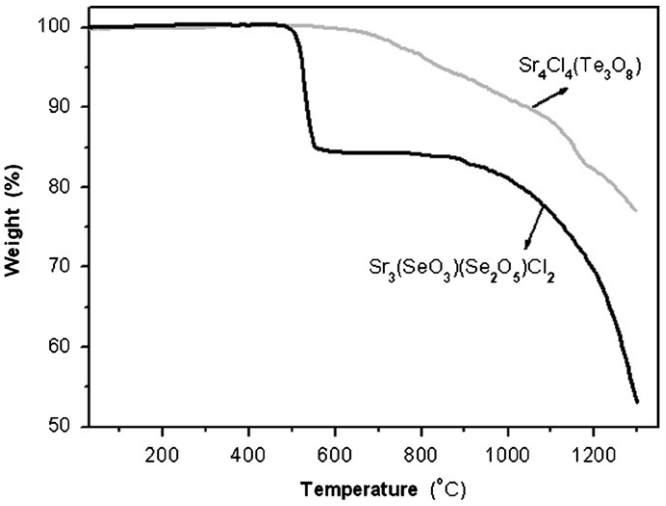

Fig. 5. TGA curves for $Sr_3(SeO_3)(Se_2O_5)Cl_2$ and $Sr_4(Te_3O_8)Cl_4$.

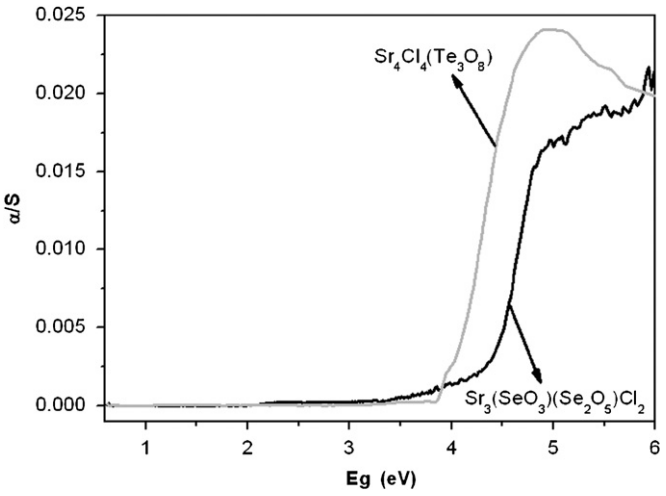

Fig. 6. Room temperature optical absorption spectra for $Sr_3(SeO_3)(Se_2O_5)Cl_2$ and $Sr_4(Te_3O_8)Cl_4$.

3.5. Theoretical studies

The calculated band structures of $Sr_3(SeO_3)(Se_2O_5)Cl_2$ and $Sr_4(Te_3O_8)Cl_4$ along the high-symmetry points of the

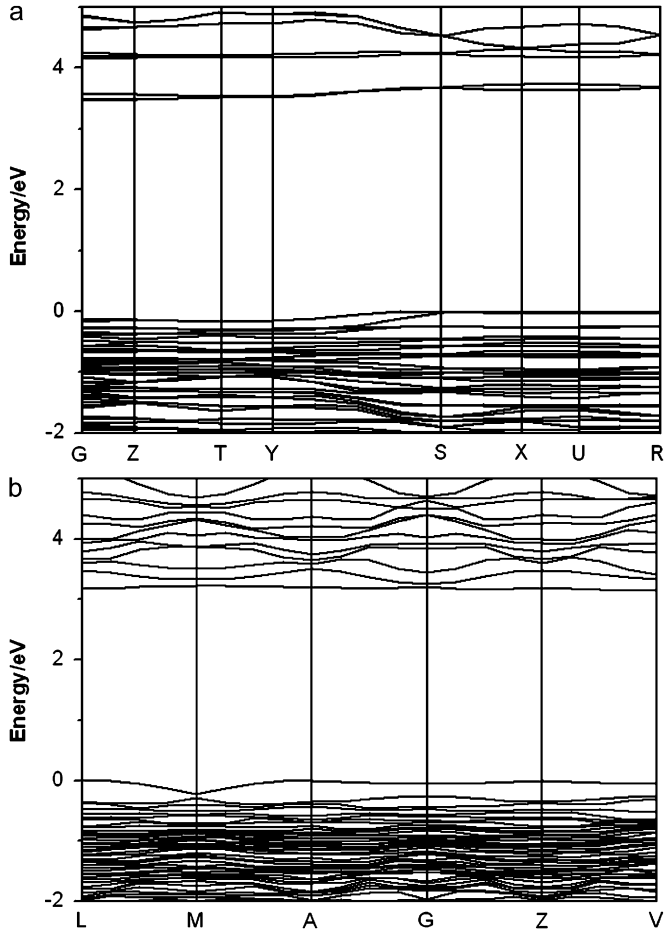

Fig. 7. Band structures of $Sr_3(SeO_3)(Se_2O_5)Cl_2$ (a) and $Sr_4(Te_3O_8)Cl_4$ (b) (bands are shown only between −2 and 5 eV for clarity, and the Fermi level is set at 0 eV).

first Brillouin zone are plotted in Fig. 7. It is found that both the top of valence bands (VBs) and the bottom of conduction bands (CBs) are very flat for both compounds. The state energies (eV) of the lowest conduction band (L-CB) and the highest valence band (H-VB) at some *k*-points are listed in Table 3. For $Sr_3(SeO_3)(Se_2O_5)Cl_2$, the lowest energy (3.47 eV) of CBs is located at the G point whereas the highest energy (−0.02 eV) of VBs is located at the U point whereas, for $Sr_4(Te_3O_8)Cl_4$, the lowest energy (3.16 eV) of CBs occurred at the V point whereas the highest energy (0 eV) of VBs is located at the L or Z point. Therefore, both compounds are indirect wide band-gap semiconductors. The calculated band gaps of 3.49 and 3.16 eV are much smaller than the experimental values of 4.4 and 4.0 eV, respectively, for Se and Te compounds. Such discrepancy is due to the limitation of DFT method that sometimes underestimates the band gap in semiconductors and insulators [64,67,68]. As a result, scissors operators of 0.9 and 0.8 eV were applied for the calculations of density-of-states (DOS) and optical properties, respectively, for the Se and Te compounds.

The bands can be assigned according to the total and partial DOS (TDOS and PDOS) as plotted in Fig. 8. The

Table 3
The state energies (eV) of the lowest conduction band (L-CB) and the highest valence band (H-VB) at some k-points of the crystal $Sr_3(SeO_3)(Se_2O_5)Cl_2$ and $Sr_4(Te_3O_8)Cl_4$

Compound	*k*-Point	L-CB	H-VB
$Sr_3(SeO_3)(Se_2O_5)Cl_2$	G (0.0, 0.0, 0.0)	3.46938	−0.11810
	Z (0.0, 0.0, 0.5)	3.47785	−0.13597
	T (−0.5, 0.0, 0.5)	3.52152	−0.16479
	Y (−0.5, 0.0, 0.0)	3.51696	−0.15859
	S (−0.5, 0.5, 0.0)	3.68861	−0.01975
	X (0.0, 0.5, 0.0)	3.63257	−0.01899
	U (0.0, 0.5, 0.5)	3.63303	−0.01677
	R (−0.5, 0.5, 0.5)	3.68996	−0.01936
$Sr_4(Te_3O_8)Cl_4$	L (−0.5, 0.0, 0.5)	3.18381	0
	M (−0.5, −0.5, 0.5)	3.22094	−0.22637
	A (−0.5, 0.0, 0.0)	3.19936	−0.00006
	G (0.0, 0.0, 0.0)	3.20274	−0.05302
	Z (0.0, −0.5, 0.5)	3.18381	0
	V (0.0, 0.00, 0.5)	3.16304	−0.05366

TDOS and PDOS of both compounds exhibit some similarities. For both compounds, the regions below the Fermi level (the Fermi level is set at the top of the valence band) can be divided into three regions. The VB lying near −31.5 eV are mainly contributions of Sr-4s, 5s states. The VBs ranging from −21.5 to −8.5 eV (−19.5 to −11.8 eV for the Te compound) are formed by the states of Sr-4p, Cl-3s, O-2s mixing with small amount of Se-4s, 4p (or Te-5s, 5p for the Te compound) states. The main contributions of VBs ranging from −7.2 eV (−10.1 eV for the Te compound) to the Fermi level (0.0 eV) are O-2p, Cl-3p and Se-4p (or Te-5p) states mixed with small amount of Se-4s (or Te-5s) and O-2s states.

The bands above the Fermi level are derived from Se-4p (or Te-5p) and O-2p sates in 3.8–6.4 and 3.5–6.5 eV, respectively, for $Sr_3(SeO_3)(Se_2O_5)Cl_2$ and $Sr_4(Te_3O_8)Cl_4$. The VBs just below the Fermi level are mainly from O-2p, Cl-3p states mixing with a small amount of the Se-4s, Se-4p (or Te-5s and Te-5p). Therefore, their optical absorptions can mainly be ascribed to the charge transitions from O-2p and Cl-3p to Se-4p (or Te-5p) states.

In addition, we also calculated the atomic site and angular momentum projected DOS of $Sr_3(SeO_3)(Se_2O_5)Cl_2$ and $Sr_4(Te_3O_8)Cl_4$ to elucidate the nature of the electronic band structure and chemical bonds. As shown in Fig. 8, it is observed that the densities of O-2p states are larger than those of Se-4s, 4p (or Te-5s, 5p) between −3.0 eV and the Fermi level, indicating that the hybridization of Se-4s, 4p (or Te-5s, 5p) with O-2p states and the weak covalent bonding between Se or Te and O atoms. The peaks of the total DOS around −31.5 and −14.8 eV are predominantly originated from Sr-4s to Sr-4p states, indicative of the ionic bonding between Sr and O or Cl atoms. The chemical bonding properties are also evident from the population analyses. For $Sr_3(SeO_3)(Se_2O_5)Cl_2$, the Mulliken bond orders for Se–O (1.651(6)−1.695(6) Å) range from 0.34 to 0.47 e, Se–O bond with 1.818(9) Å has a much smaller bond

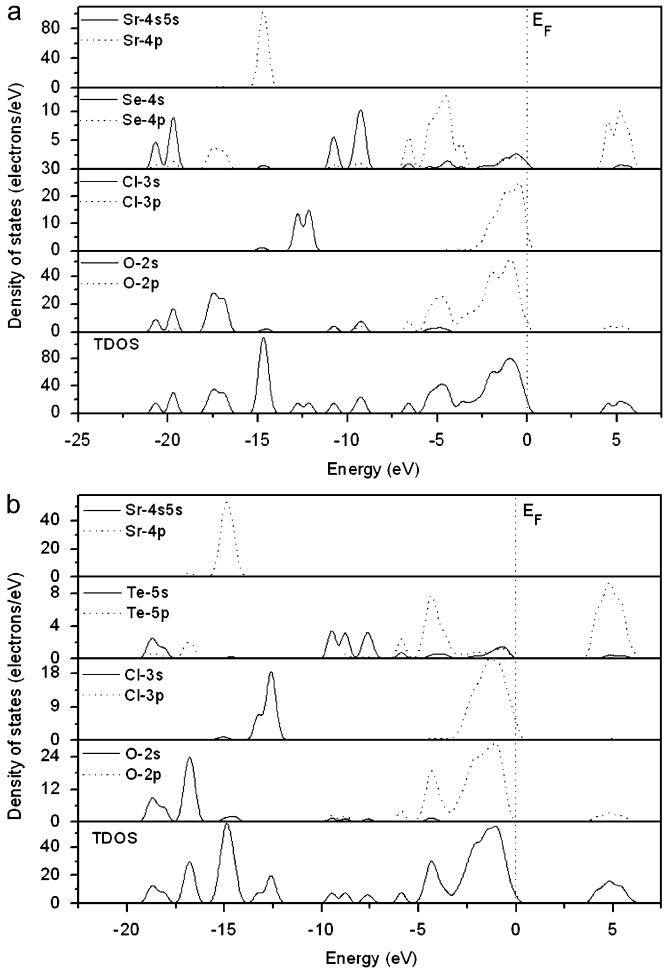

Fig. 8. Total and partial DOS of $Sr_3(SeO_3)(Se_2O_5)Cl_2$ (a) and $Sr_4(Te_3O_8)Cl_4$ (b). The energies less than −25.0 eV are omitted for clarity, the Fermi level is set at 0 eV.

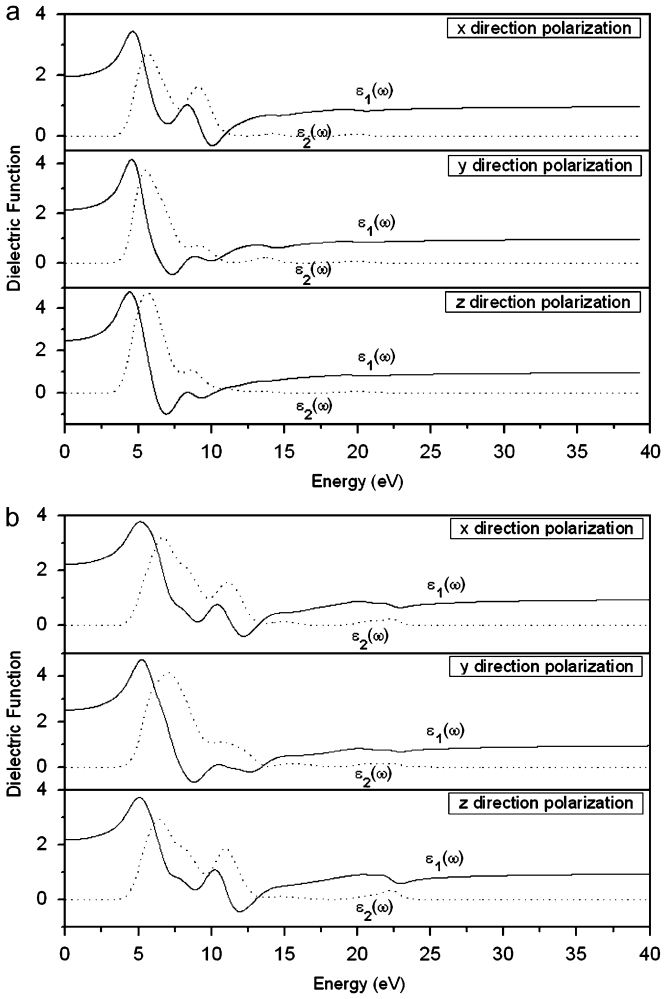

Fig. 9. Calculated real and imaginary parts of dielectric functions of $Sr_3(SeO_3)(Se_2O_5)Cl_2$ (a) and $Sr_4(Te_3O_8)Cl_4$ (b) in different polarization directions.

order of 0.15 and 0.21 e. The bond orders for the Sr–O and Sr–Cl interactions are in the range of 0.05–0.12 and 0.14*e*, respectively. For $Sr_4(Te_3O_8)Cl_4$, the Mulliken bond orders of the short Te–O bonds (1.851(5)−1.896(8) Å) fall in the range of 0.30–0.48*e* whereas Te–O bonds with longer distances of 2.114(8) and 2.130(9) Å) have a much smaller bond order of 0.11 and 0.13*e*, respectively. The bond orders for the Sr–O and Sr–Cl interactions are in the range of 0.07–0.12 and 0.14–0.19*e*, respectively. Accordingly, we can conclude that the covalent character of the Se–O or Te–O bond is larger than that of the Sr–O and Sr–Cl bonds in both compounds.

To evaluate and assign the observed absorption spectra, we also examined the linear optical response properties of $Sr_3(SeO_3)(Se_2O_5)Cl_2$ and $Sr_4(Te_3O_8)Cl_4$ crystals. The calculated imaginary part $\varepsilon_2(\omega)$ and the real part $\varepsilon_1(\omega)$ of the frequency-dependent dielectric functions are in Fig. 9. It is found from the dispersion of the calculated $\varepsilon_2(\omega)$ spectra that the maximum absorption peaks are located at about 6.65 eV (187 nm), 7.06 eV (176 nm), and 6.43 eV (193 nm) for $Sr_3(SeO_3)(Se_2O_5)Cl_2$, and about 5.63 eV (220 nm), 5.48 eV (226 nm), and 5.59 eV (222 nm) for $Sr_4(Te_3O_8)Cl_4$ in *x*, *y*, and *z* polarization directions, respectively. These are comparable to the experimental ones at about 5.24 and 5.02 eV, respectively, for the Se and Te compounds, both of which are contribution from the charge transfers from O-2p and Cl-3p to Se-4p or Te-5p states according to the above DOS analysis. It is noted that the absorption peaks locate at a lower energy for the powder sample than for the single crystal and the UV transparent widths are smaller for the powder samples compared to these of the single crystals [64,69]. The crystals show no absorption when the wavelengths are larger than 303 and 365 nm or photon energies less than 4.1 and 3.4 eV, respectively, for the Se and Te compounds. The observed ultraviolet edge of cut-off is at about 282 and 299 nm for polycrystalline power sample of Se and Te compounds, respectively (see Supporting Materials). Hence, our calculated value is reasonable.

Dielectric constant is an important optical property. It is a measurement of how fast light travels in a medium. The lower is the dielectric constant, the faster the speed of light. The calculated dielectric constants of static case $\varepsilon(0)$ are

about 2.2432, 2.5122 and 2.1921 for $Sr_3(SeO_3)(Se_2O_5)Cl_2$, and 1.9641, 2.1451, and 2.4933 for $Sr_4(Te_3O_8)Cl_4$ in *x*-, *y*-, and *z*-directions, respectively. The dispersion curves of refractive index are also calculated by the relation of $n^2(\omega)=\varepsilon(\omega)$, and the refractive indices of n_x, n_y, and n_z are 1.51, 1.60, and 1.49 for $Sr_3(SeO_3)(Se_2O_5)Cl_2$, and 1.41, 1.48, and 1.60 for $Sr_4(Te_3O_8)Cl_4$ at a wavelength of 1064 nm, respectively. The refractive indices of $Sr_3(SeO_3)(Se_2O_5)Cl_2$ and $Sr_4(Te_3O_8)Cl_4$ or other metal selenites or tellurites crystals have not been measured and reported, and therefore, our results can only be compared with corresponding metal selenates and tellurite glasses reported. It is reported that the observed refractive index of triclinic rubidium hydrogen selenate (generally 1.5–1.6) is comparable to our calculations [70]. While comparable to metal tellurite glasses (generally 2.1 at 400–700 nm) [71,72], our calculated results are underestimate about 20%.

4. Conclusion

In conclusion, the syntheses, crystal and band structures, and optical properties of $Sr_3(SeO_3)(Se_2O_5)Cl_2$ and $Sr_4(Te_3O_8)Cl_4$ have been described. $Sr_3(SeO_3)(Se_2O_5)Cl_2$ features a 3D structure in which the Sr^{2+} cations are bridged by Cl^-, SeO_3^{2-}, and $Se_2O_5^{2-}$ anions, whereas, the structure of $Sr_4(Te_3O_8)Cl_4$ is a 3D network composed of strontium tellurium(IV) oxide slabs and strontium chloride layers. It is found that the tellurium(IV) compounds usually display different structures from those of the corresponding selenium(IV) ones due to the different coordination geometries around Se(IV) and Te(IV) atoms and the polymerization of the TeO_x ($x=3$, 4, 5) groups. Both compounds are wide indirect band gap semiconductors based on experimental measurements and electronic band structure calculations. It is observed that the sharp absorption peaks are at about 237 and 247 nm, respectively, for Se and Te compounds, which mainly originates from charge transfer from O-2p and Cl-3p to Se-4p or Te-5p states. We are currently exploring other AE selenium(IV) or tellurium(IV) oxychlorides with novel structures and interesting optical properties.

Acknowledgments

The authors gratefully acknowledge the support from the Knowledge Innovation Program of the Chinese Academy of Sciences and the National Natural Science Foundation of China (Nos. 20731006 and 20573113).

Appendix A. Supplementary Materials

Supplementary data associated with this article can be found in the online version at doi:10.1016/j.jssc.2007.12.007.

References

[1] M.S. Wickleder, Chem. Rev. 102 (2002) 2011–2087 (and references therein).
[2] V.P. Verma, Thermochim. Acta 327 (1999) 63–102 (and references therein).
[3] J. Nye, Physical Properties of Crystals, Oxford University Press, Oxford, 1957.
[4] H.S. Ra, K.M. Ok, P.S. Halasyamani, J. Am. Chem. Soc. 125 (2003) 7764–7765.
[5] J. Goodey, J. Broussard, P.S. Halasyamani, Chem. Mater. 14 (2002) 3174–3180.
[6] P.S. Halasyamani, Chem. Mater. 16 (2004) 3586–3592.
[7] E.O. Chi, K.M. Ok, Y. Porter, P.S. Halasyamani, Chem. Mater. 18 (2006) 2070–2074.
[8] K.M. Ok, P.S. Halasyamani, Chem. Mater. 18 (2006) 3176–3183.
[9] W.T.A. Harrison, L.L. Dussack, A.J. Jacobson, Inorg. Chem. 33 (1994) 6043–6049.
[10] Y. Porter, K.M. Ok, N.S.P. Bhuvanesh, P.S. Halasyamani, Chem. Mater. 13 (2001) 1910–1915.
[11] P.S. Berdonosov, S.Yu. Stefanovitch, V.A. Dolgikh, J. Solid State Chem. 149 (2000) 236–241.
[12] P.S. Berdonosov, D.O. Charkin, A.M. Kusainova, C.H. Hervoches, V.A. Dolgikh, P. Lightfoot, Solid State Sci. 2 (2000) 553–562.
[13] M.P. Minimol, K. Vidyasagar, Inorg. Chem. 44 (2005) 9369–9373.
[14] V. Balraj, K. Vidyasagar, Inorg. Chem. 37 (1998) 4764–4774.
[15] W.T.A. Harrison, L.L. Dussack, A.J. Jacobson, J. Solid. State Chem. 125 (1996) 234–242.
[16] M. Johnsson, K.W. Törnroos, F. Mila, P. Millet, Chem. Mater. 12 (2000) 2853–2857.
[17] M. Johnsson, K.W. Törnroos, P. Lemmens, P. Millet, Chem. Mater. 15 (2003) 68–73.
[18] R. Becker, M. Johnsson, R.K. Kremer, H.H. Klauss, P. Lemmens, J. Am. Chem. Soc. 128 (2006) 15469–15475.
[19] R. Takagi, M. Johnsson, V. Gnezdilov, R.K. Kremer, W. Brenig, P. Lemmens, Phys. Rev. B 74 (2006) 014413–014418.
[20] M. Johnsson, K.W. Törnroos, Solid State Sci. 5 (2003) 263–266.
[21] P. Millet, B. Bastide, M. Johnsson, Solid State Commun. 113 (2000) 719–723.
[22] B. Bastide, P. Millet, M. Johnsson, J. Galy, Mater. Res. Bull. 35 (2000) 847–855.
[23] R. Becker, M. Johnsson, Solid State Sci. 6 (2004) 519–522.
[24] P. Millet, B. Bastide, V. Pashchenko, S. Gnatchenko, V. Gapon, Y. Ksari, A. Stepanov, J. Mater. Chem. 11 (2001) 1152–1157.
[25] J. Wontcheu, T. Schleid, J. Solid State Chem. 171 (2003) 429–433.
[26] H.L. Jiang, J.G. Mao, Inorg. Chem. 45 (2006) 717–721.
[27] H.L. Jiang, J.G. Mao, Inorg. Chem. 45 (2006) 7593–7599.
[28] J. Yeon, P. S. Halasyamani, I. V. Kityk, Mater. Lett. 62 (2008) 1082.
[29] K.M. Ok, P.S. Halasyamani, Inorg. Chem. 43 (2004) 4248–4253.
[30] K.M. Ok, J. Orzechowski, P.S. Halasyamani, Inorg. Chem. 43 (2004) 964–968.
[31] M.G. Johnston, W.T.A. Harrison, Acta Crystallogr. E 58 (2002) i49–i51.
[32] D. Hottentot, B.O. Loopstra, Acta Crystallogr. C 39 (1983) 1600–1602.
[33] C.R. Feger, J.W. Kolis, Inorg. Chem. 37 (1998) 4046–4051.
[34] R. Takagi, M. Johnsson, Acta Crystallogr. C 62 (2006) i38–i40.
[35] R. Takagi, M. Johnsson, Acta Crystallogr. C 61 (2005) i106–i108.
[36] W.W.M. Wendlandt, H.G. Hecht, Reflectance Spectroscopy, Wiley, New York, 1966.
[37] CrystalClear ver. 1.3.5. Rigaku Corp., Woodlands, TX, 1999.
[38] G.M. Sheldrick, SHELXTL, Crystallographic Software Package, SHELXTL, Version 5.1, Bruker-AXS, Madison, WI, 1998.
[39] M.D. Segall, P.L.D. Lindan, M.J. Probert, C.J. Pickard, P.J. Hasnip, S.J. Clark, M.C. Payne, J. Phys.: Condens. Matter 14 (2002) 2717–2744.
[40] V. Milman, B. Winkler, J.A. White, C.J. Pickard, M.C. Payne, E.V. Akhmatskaya, R.H. Nobes, Int. J. Quantum Chem. 77 (2000) 895–910.
[41] M. Segall, P. Linda, M. Probert, C. Pickard, P. Hasnip, S. Clark, M. Payne, Materials Studio CASTEP, version 2.2, 2002.

[42] J.P. Perdew, K. Burke, M. Ernzerhof, Phys. Rev. Lett. 77 (1996) 3865–3868.
[43] J.S. Lin, A. Qteish, M.C. Payne, V. Heine, Phys. Rev. B 47 (1993) 4174–4180.
[44] D.R. Hamann, M. Schluter, C. Chiang, Phys. Rev. Lett. 43 (1979) 1494–1497.
[45] J.R. Macdonald, M.K. Brachman, Rev. Mod. Phys. 28 (1956) 393–422.
[46] S.M. Loureiro, C. Felser, Q. Huang, R.J. Cava, Chem. Mater. 12 (2000) 3181–3185.
[47] A.L. Hector, J. Hutchings, R.L. Needs, M.F. Thomas, M.T. Weller, J. Mater. Chem. 11 (2001) 527–532.
[48] I.D. Brown, D. Altermatt, Acta Crystallogr. B 41 (1985) 244–247.
[49] N.E. Brese, M. O'Keeffe, Acta Crystallogr. B 47 (1991) 192–197.
[50] J. Galy, G. Meunier, S. Andersson, A. Åström, J. Solid State Chem. 13 (1975) 142–159.
[51] G. Giester, C.L. Lengauer, Monatsh. Chem. 129 (1998) 445–454.
[52] P.G. Jones, E. Schwarzmann, G.M. Sheldrick, H. Timpe, Z. Naturforsch. B 36 (1981) 1050–1051.
[53] M. Koskenlinna, J. Valkonen, Acta Chem. Scand. 31 (1977) 638–640.
[54] M. Koskenlinna, J. Valkonen, Acta Chem. Scand. 31 (1977) 457–460.
[55] M. Wildner, M. Andrut, J. Solid State Chem. 135 (1998) 70–77.
[56] H. Muilu, J. Valkonen, Acta Chem. Scand. A 41 (1987) 183–189.
[57] R.E. Morris, A.K. Cheetham, Chem. Mater. 6 (1994) 67–69.
[58] M. Stancheva, R. Petrova, J. Macicek, Acta Crystallogr. C 54 (1998) 699–701.
[59] H.-L. Jiang, E. Ma, J.-G. Mao, Inorg. Chem. 46 (2007) 7012–7023.
[60] G.B. Nikiforov, A.M. Kusainova, P.S. Berdonosov, V.A. Dolgikh, P. Lightfoot, J. Solid State Chem. 146 (1999) 473–477.
[61] S.F. Meier, T. Schleid, Z. Anorg. Allg. Chem. 629 (2003) 1575–1580.
[62] K.-M. Ok, P.S. Halasyamani, Chem. Mater. 13 (2001) 4278–4284.
[63] I. Ijjaali, C. Flaschenriem, J.A. Ibers, J. Alloys Compds. 354 (2003) 115–119.
[64] H.L. Jiang, F. Kong, J.G. Mao, J. Solid State Chem. 180 (2007) 1764–1769.
[65] Y. Porter, P.S. Halasyamani, Inorg. Chem. 42 (2003) 205–209.
[66] K.M. Ok, P.S. Halasyamani, Chem. Mater. 14 (2002) 2360–2364.
[67] R.W. Godby, M. Schluther, L.J. Sham, Phys. Rev. B 36 (1987) 6497–6500.
[68] C.M.I. Okoye, J. Phys.: Condens. Matter 15 (2003) 5945–5958.
[69] J. Zhu, W.-D. Cheng, D.-S. Wu, H. Zhang, Y.-J. Gong, H.-N. Tong, D. Zhao, Eur. J. Inorg. Chem. (2007) 285–290.
[70] L. Guilbert, J.P. Salvestrini, P. Kolata, F.X. Abrial, M.D. Fontana, Z. Czapla, J. Opt. Soc. Am. B 15 (1998) 1009–1016.
[71] S. Inoue, A. Nukui, K. Yamamoto, T. Yano, S. Shibata, M. Yamane, J. Non-Cryst. Solids 324 (2003) 133–141.
[72] E. Yousef, M. Hotzel, C. Rűssel, J. Non-Cryst. Solids 342 (2004) 82–88.